Acta Pharmaceutica Sinica B 2023;13(9):3945–3955

Chinese Pharmaceutical Association
Institute of Materia Medica, Chinese Academy of Medical Sciences

Acta Pharmaceutica Sinica B

www.elsevier.com/locate/apsb
www.sciencedirect.com

SHORT COMMUNICATION

# Antitumor synergism between PAK4 silencing and immunogenic phototherapy of engineered extracellular vesicles

**Mei Lu[a,b,†], Haonan Xing[b,c,†], Wanxuan Shao[a], Pengfei Wu[a], Yuchuan Fan[a], Huining He[d], Stefan Barth[e], Aiping Zheng[c], Xing-Jie Liang[b,*], Yuanyu Huang[a,*]**

[a]*Advanced Research Institute of Multidisciplinary Science, School of Life Science, School of Medical Technology, Key Laboratory of Molecular Medicine and Biotherapy, Key Laboratory of Medical Molecule Science and Pharmaceutics Engineering, Beijing Institute of Technology, Beijing 100081, China*
[b]*Chinese Academy of Sciences (CAS) Key Laboratory for Biomedical Effects of Nanomaterials and Nanosafety, CAS Center for Excellence in Nanoscience, National Center for Nanoscience and Technology of China, Beijing 100190, China*
[c]*State Key Laboratory of Toxicology and Medical Countermeasures, Beijing Institute of Pharmacology and Toxicology, Beijing 100850, China*
[d]*Tianjin Key Laboratory on Technologies Enabling Development of Clinical Therapeutics and Diagnostics, School of Pharmacy, Tianjin Medical University, Tianjin 300070, China*
[e]*South African Research Chair in Cancer Biotechnology, Institute of Infectious Disease and Molecular Medicine (IDM), Department of Integrative Biomedical Sciences, Faculty of Health Sciences, University of Cape Town, Cape Town 7925, South Africa*

Received 1 January 2023; received in revised form 4 March 2023; accepted 23 March 2023

**KEY WORDS**

Antitumor synergism;
Combined cancer immunotherapy;
p21-activated kinase 4;
RNA interference;

**Abstract** Immunotherapy has revolutionized the landscape of cancer treatment. However, single immunotherapy only works well in a small subset of patients. Combined immunotherapy with antitumor synergism holds considerable potential to boost the therapeutic outcome. Nevertheless, the synergistic, additive or antagonistic antitumor effects of combined immunotherapies have been rarely explored. Herein, we established a novel combined cancer treatment modality by synergizing p21-activated kinase 4 (PAK4) silencing with immunogenic phototherapy in engineered extracellular vesicles (EVs) that were

*Corresponding authors.
E-mail addresses: liangxj@nanoctr.cn (Xing-Jie Liang), yyhuang@bit.edu.cn (Yuanyu Huang).
[†]These authors made equal contribution to this work.
Peer review under the responsibility of Chinese Pharmaceutical Association and Institute of Materia Medica, Chinese Academy of Medical Sciences.

https://doi.org/10.1016/j.apsb.2023.03.020
2211-3835 © 2023 Chinese Pharmaceutical Association and Institute of Materia Medica, Chinese Academy of Medical Sciences. Production and hosting by Elsevier B.V. This is an open access article under the CC BY-NC-ND license (http://creativecommons.org/licenses/by-nc-nd/4.0/).

Immunogenic phototherapy;
Extracellular vesicles;
Immune infiltration;
CompuSyn

fabricated by coating M1 macrophage-derived EVs on the surface of the nano-complex cores assembled with siRNA against PAK4 and a photoactivatable polyethyleneimine. The engineered EVs induced potent PAK4 silencing and robust immunogenic phototherapy, thus contributing to effective antitumor effects *in vitro* and *in vivo*. Moreover, the antitumor synergism of the combined treatment was quantitatively determined by the CompuSyn method. The combination index (CI) and isobologram results confirmed that there was an antitumor synergism for the combined treatment. Furthermore, the dose reduction index (DRI) showed favorable dose reduction, revealing lower toxicity and higher biocompatibility of the engineered EVs. Collectively, the study presents a synergistically potentiated cancer treatment modality by combining PAK4 silencing with immunogenic phototherapy in engineered EVs, which is promising for boosting the therapeutic outcome of cancer immunotherapy.

© 2023 Chinese Pharmaceutical Association and Institute of Materia Medica, Chinese Academy of Medical Sciences. Production and hosting by Elsevier B.V. This is an open access article under the CC BY-NC-ND license (http://creativecommons.org/licenses/by-nc-nd/4.0/).

## 1. Introduction

Immunotherapy has achieved remarkable success in combatting cancers. However, cancer cells exploit various tactics to adapt, evade and even resist immune attack[1]. Single immunotherapy frequently leads to treatment failure due to different adaptive immune resistance, and only a small fraction of patients (*i.e.*, 10%−30%) benefit from the treatment[2]. Nowadays, various strategies have been developed to enhance the response rate of cancer immunotherapy[1]. For example, patients are generally stratified as potential responders versus no-responders, and only responders receive specific immunotherapy. Another promising strategy is to develop combined immunotherapy, especially for that with synergistic antitumor effects, to promote proper treatment modalities are synergized to maximize the therapeutic outcome[3−5].

Tumor-cell-intrinsic immune exclusion and the poor immunogenicity of the tumor microenvironment (TME) are two primary mechanisms accounting for the low response rate of cancer immunotherapy[6,7]. P21-activated kinases 4 (PAK4) is a well-known driver for the proliferation, development, and progression of various tumor malignancies, such as melanomas, colorectal carcinoma, breast cancer, and pancreatic cancer[8,9]. More recently, it has been identified that PAK4 represents a key tumor "guard" for immune exclusion. PAK4 could promote the phosphorylation and nuclear translocation of the transcription factor $\beta$-catenin, thus activating the Wnt/$\beta$-catenin pathway, an oncogenic signaling pathway involving in exclusion of tumor-infiltrating immune cells[10,11]. To this end, downregulation of PAK4 expression can not only inhibit the survival of cancer but also can boost intratumoral immune infiltration. To trigger potent antitumor effects, effective PAK4 silencing should be combined with strategies that can enhance the immunogenicity of TME. Phototherapy is typically able to induce immunogenic cell death (ICD) and thus directly kill cancer cells. Additionally, the lysed tumor cells can in turn release damage-associated molecular patterns (DAMPs) and tumor antigens. These signals can further increase tumor immunogenicity and promote the maturing of antigen-presenting cells such as dendritic cells (DCs), which finally results in the activation of cytotoxic $CD8^+$ T cells[12−14]. During the last few years, combining immunogenic phototherapy with other immunotherapies has attracted ever-growing attention[5,15]. However, the synergistic, additive, and antagonistic antitumor effect of the combined treatment has been rarely explored.

Extracellular vesicles (EVs) are naturally occurring membrane-enclosed vesicles secreted by almost all cell types. Owing to the role of natural RNA nanocarriers, EVs have sparked intensive interest in the delivery of diverse nucleic acid therapeutics, including siRNAs, miRNAs, mRNAs, ASOs, and other types of RNAs[16−19]. In addition, several pharmaceuticals in the EV industry, such as Codiak Biosciences and EVOX Therapeutics, have harnessed EVs for nucleic acid therapy. EVs are characterized by numerous favorable characteristics for therapeutic delivery, such as excellent biocompatibility, low immunogenicity, protection of nucleic acid therapeutics, intrinsic targeting capacity, circulation stability, the capacity of crossing biological membranes, and the ability to gain direct cytosolic delivery[18,20−22]. Moreover, EVs derived from specific cell types possess some unique characteristics analogous to their parental cells. For example, M1 macrophages possess innate inflammation-directed tumor accumulation properties. Due to cellular originality, EVs derived from M1 macrophages also possess the tumor tropism property[23,24]. However, the clinical translation of EVs is still constrained by low isolation yield and loading efficiency[25,26]. Under this circumstance, engineering bioinspired EV-like nanosystems can simultaneously take advantage of the unique properties of EVs and the facile preparation and cargo loading of synthetic nanoparticles[27−30].

In this study, a synergistic cancer treatment modality was established by combining PAK4 silencing with immunogenic phototherapy in engineered EVs. To this end, siRNA against the target PAK4 (siPAK4) was complexed with a chlorin e6 (Ce6)-conjugated, thioketal-linked polyethyleneimine (TPC) to obtain the photoactivatable nano-complexes (TPCS). Then, TPCS was encapsulated by M1 macrophage-derived EVs to generate the engineered EVs (TPCS@EV). TPCS@EV could simultaneously silence the expression of PAK4 and induce robust immunogenic phototherapy *in vitro* and *in vivo*, thereby, contributing to effective antitumor effects. As quantitively confirmed by using the CompuSyn software (ComboSyn, Inc., Paramus, NJ), the combined treatment of the engineered EVs exhibited antitumor synergism between PAK4 silencing and immunogenic phototherapy, thus contributing to synergistically potentiated therapeutic outcomes (Fig. 1).

## 2. Materials and methods

### 2.1. Materials

Lipofectamine 2000 (Lipo 2000) (Thermo Fisher Scientific, Waltham, USA); siPAK4, scramble siRNA (siNC) and Cyanine 5-

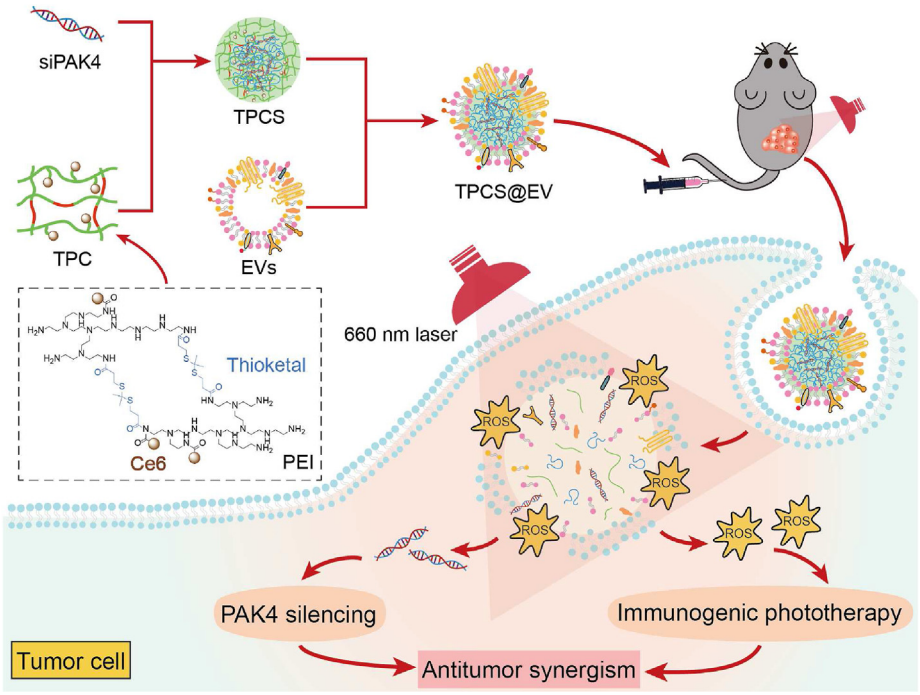


**Figure 1** Schematic depiction of the synergistic cancer treatment modality of engineered EVs (TPCS@EV) by combining PAK4 silencing with immunogenic phototherapy. siRNA against the drug target PAK4 (siPAK4) was complexed with a chlorin e6 (Ce6)-conjugated, reactive oxygen species (ROS)-degradable polyethyleneimine (TPC) to form the nano-complexes (TPCS). Subsequently, the TPCS nano-complex cores were encapsulated by M1 macrophage-derived EVs to construct the engineered EVs (TPCS@EV). TPCS@EV could elicit potent PAK4 silencing and robust immunogenic phototherapy, thus contributing to synergistically boosted antitumor therapeutic outcomes.

labeled siNC (Cy5 siNC) (Suzhou Ribo Life Science, Jiangsu, China); branched PEI (1.8 kDa) and Ce6 (J&K Chemical, Shanghai, China); 2,7-dichloro-dihydro-fluorescein diacetate (DCFH-DA) (Yeasen, Shanghai, China); Annexin V-FITC/propidium iodide (Annexin V-FITC/PI) staining kit (Yeasen, Shanghai, China); 3-(4,5-dimethylthiazol-2-yl)-2,5-diphenyltetrazolium bromide (MTT) (Sigma−Aldrich, St. Louis, USA); anti-PAK4 antibody (14685-1-AP), anti-calreticulin (CRT) antibody and anti-$\beta$-Actin antibody (20536-1-AP) (Proteintech, Chicago, USA); horseradish peroxidase-conjugated secondary antibody (ZSGB-Bio, Beijing, China); mouse high mobility group box 1 protein (HMGB1) ELISA kit (Nanjing Jin Yibai Biotechnology, Nanjing, China); adenosine triphosphate (ATP) assay kit (Beyotime Biotechnology, Shanghai, China).

### 2.2. *Cell culture and animals*

RAW264.7, B16F10, and CT26 cells expressing firefly luciferase (CT26-Luc) cells were obtained from the Institute of Basic Medical Sciences, Chinese Academy of Medical Sciences. RAW264.7 and B16F10 cells were maintained in DMEM supplemented with 10% fetal bovine serum (FBS) and 1% penicillin-streptomycin, while CT26-Luc cells were cultured in RPMI 1640 supplemented with 10% FBS and 1% penicillin-streptomycin. Cultures were maintained in a humidified atmosphere of 5% $CO_2$ at 37 °C.

C57BL/6J mice (female, 6−8 weeks) and BALB/c mice (female, 6−8 weeks) were bought from Beijing Vital River Laboratory Animal Technology Co., Ltd. All animal experiments were performed under the guidelines of the Institutional Animal Care and Use Committee (IACUC) of Beijing Institute of Technology (approval number, BIT-EC-SCXK (Beijing) 2016-0006-M-202016).

### 2.3. *Preparation of the engineered EVs*

The engineered EVs (TPCS@EV) were prepared by coating M1 macrophage-derived EVs on the surface of TPCS nano-complex cores formed between siPAK4 and Ce6-conjugated, thioketal-linked polyethyleneimine (TPC). EVs were isolated by ultracentrifugation at 100,000 $\times g$, 4 °C for 90 min using an Optima XPN-100 centrifuge (Beckman Coulter, Germany). The isolated EVs were subjected to a hypotonic treatment to isolate the EV membrane through incubation with a mixture buffer consisting of Tris (2 mmol/L), MgCl2 (1 mmol/L), KCl (1 mmol/L), and 1% (*v*/*v*) protease inhibitor cocktail at 4 °C overnight[31]. The identity of EVs was evaluated by western blot, transmission electron microscopy (HT7700, Hitachi, Japan) imaging, nanoparticle tracking analysis (ZetaView PMX120, Particle Metrix, Germany), and CytoFLEX Flow Cytometer (Beckman, Germany). The photoactivatable polyethyleneimine (TPC) was synthesized by cross-linking PEI with thioketal and conjugating with Ce6, according to our previous work[32]. TPC was complexed with siPAK4 to obtain the TPCS nano-complex cores at a weight ratio of 10:1 between TPC and siPAK4. Encapsulation of TPCS nano-complex cores by EVs was achieved by using an extrusion approach reported previously[31]. Briefly, EVs were mixed homogenously with TPCS nano-complexes at an optimized weight ratio between EVs and TPCS of 1:1. The mixture was then physically co-extruded through a 200 nm polycarbonate membrane for 11 passes using a mini-extruder (Avestin LiposoFast LF1, Canada). The encapsulation of TPCS by EVs was characterized by using several

approaches, including confocal laser scanning microscopy (CLSM, Zeiss Z-760, Germany), NanoView (ExoView R200, USA), transmission electron microscopy (TEM), dynamic light scattering (DLS) and sodium dodecyl sulfate-polyacrylamide gel electrophoresis (SDS-PAGE). To characterize the storage stability, the particle size of TPCS@EV and TPCS nanoparticles in phosphate buffer saline (PBS) before and after storing at room temperature away from light for 24 h was measured. The encapsulation efficiency of siPAK4 by TPCS@EV was determined by using the Quant-iT RiboGreen RNA assay. To characterize the reactive oxygen species (ROS)-responsive characteristic, the morphology and siRNA release properties of TPCS@EV with or without laser irradiation were measured by using TEM and agarose gel retardation assay, respectively. The tumor tropism properties of TPCS@EV, TPCS, and EVs were evaluated in B16F10 tumor-bearing mice by using *in vivo* fluorescence imaging (PerkinElmer, USA).

### 2.4. Determination of PAK4 silencing in vitro

First, the cellular uptake of TPCS@EV was examined. B16F10 were seeded in glass-bottom dishes ($5 \times 10^4$ cells/dish) and cultured overnight. Cells were individually transfected with free Cy5 siNC, and Cy5 siNC-loaded TPCS and TPCS@EV for 4 h at a siRNA concentration of 100 nmol/L. Then, cells were stained with Hoechst 33342 and observed by CLSM. The PAK4 silencing activity of TPCS@EV was determined by using quantitative real-time PCR (qRT-PCR) and Western blot. B16F10 cells were seeded in 6-well plates at a density of $2 \times 10^5$ cells/well. The culture medium was discarded after culturing for 24 h, and opti-MEM supplemented with $TPCS^{siNC}$@EV or TPCS@EV nanoparticles with a final siRNA concentration of 100 nmol/L was added. After incubation at 37 °C for 4 h, a fresh complete medium was used to replace opti-MEM. Cells in photo-treatment groups were subjected to 660 nmol/L laser irradiation (0.1 W/cm$^2$, 2 min). After incubation for another 44 h, the mRNA and protein levels of PAK4 were determined by qRT-PCR and western blot, respectively.

For qRT-PCR analysis, the total RNA in different groups was isolated with TRIzol reagent (Sigma-Aldrich), reversely transcribed with TransScript cDNA Synthesis SuperMix (TransGen Biotech), and subjected to PCR amplification with PCR SuperMix (YEASEN), according to the manufacturer's instructions. The stable housekeeping gene GAPDH was adopted as the endogenous reference. The used primers included PAK4 (F): 5′-CGCCAAGCCGATGAGTAAC-3′, PAK4 (R): 5′-AGGGCCTTAGCACAGAGTTT-3′, GAPDH (F): 5′-AACTTTGGCATTGTGGAAGGGCTC-3′, GAPDH (R): 5′-TGGAAGAGTGGGAGTTGCTGTTGA-3′.

For western blot examination, total protein was separated by SDS-PAGE and electrotransferred to a nitrocellulose membrane. After blocking with 5% skimmed milk, the membranes were individually incubated with PAK4 and $\beta$-Actin antibodies at 4 °C overnight. Afterwards, the membranes were washed three times and incubated with horseradish peroxidase-conjugated secondary antibody at room temperature for 1 h. Protein bands were visualized by a chemiluminescence approach.

### 2.5. Measurement of intracellular ROS level

The intracellular ROS level was examined by CLSM. B16F10 cells were seeded in glass-bottom dishes ($5 \times 10^4$ cells/dish) and cultured for 24 h. Cells were then transfected with TPCS or TPCS@EV for 4 h at a siRNA concentration of 100 nmol/L. After the transfection procedure, the culture medium was replaced by a fresh complete culture medium, and cells in photo-treatment groups were subjected to laser irradiation (660 nmol/L, 0.1 W/cm$^2$) for 2 min. Thereafter, the intracellular ROS was detected by using DCFH-DA (10 μmol/L) as the ROS probe, according to the manufacturer's instructions. Subsequently, cells were stained with Hoechst 33342 and observed by CLSM.

### 2.6. Examination of immunogenic cell death cascade in vitro

For CLSM examination of CRT exposure, B16F10 cells were seeded in glass-bottom dishes ($5 \times 10^4$ cells/dish) and cultured for 24 h. Cells were transfected with TPCS@EV at a siRNA concentration of 100 nmol/L for 4 h. After being irradiated with 660 nmol/L laser (0.1 W/cm$^2$, 2 min), the cells were further incubated for 2 h and probed with CRT antibody (Proteintech, USA). After washing three times, cells were incubated with Alexa Fluor 488-conjugated secondary antibody (ZSGB-Bio, China) at room temperature for 1 h followed by a washing step. The cells were then stained with Hoechst 33342 and observed by CLSM (Zeiss Z-760, Germany). For western blot analysis, cells were seeded in 12-well plates and cultured for 24 h. Cell transfection was performed according to the above method. The expression of CRT was analyzed by probing with CRT antibody. The detailed western blot protocol was the same as that mentioned in Section 2.4. For determination of the extracellular level of HMGB1 and CRT, cells were transfected as described above. Afterwards, the conditioned media were collected and analyzed by using commercial mouse HMGB1 ELISA and ATP assay kits, according to the manufacturer's instructions, respectively.

### 2.7. PAK4 silencing and immunogenic cell death (ICD) cascade in vivo

To analyze PAK4 silencing and ICD cascade *in vivo*, B16F10 cells ($1 \times 10^6$) were inoculated into the right flank of C57BL/6J mice (female, 6−8 weeks). Mice were intravenously injected with PBS and TPCS@EV after the tumor volume reached approximately 80 mm$^3$ ($n = 3$). Mice were subjected to a total of 4 injections once every other day at an equal siRNA dosage of 1 mg/kg. The tumor tissues of mice in TPCS@EV plus photo-treatment were irradiated with 660 nmol/L laser (0.2 W/cm$^2$, 10 min) after 8 h post-injection. Mice were euthanized on Day 22 after tumor inoculation and tumor tissues were harvested. The total RNA and protein were isolated to determine the level of PAK4 by qRT-PCR and western blot, according to the method described in Section 2.4. Frozen sections of tumor tissues were prepared for immunofluorescence analysis of CRT exposure.

### 2.8. Antitumor activity in vitro

The antiproliferative effect of TPCS@EV was evaluated by measuring cell confluence using the Operetta CLS Live Cell Analysis System. B16F10 and CT26-Luc cells were cultured in 96-well plates ($4 \times 10^3$ cells/well) overnight. Subsequently, cells were transfected with TPCS@EV for 4 h at a siRNA concentration of 100 nmol/L. After replacing the culture medium with a fresh complete medium, cells in the photo-treatment group were subjected to laser irradiation (660 nmol/L, 0.1 W/cm$^2$) for 2 min, and then maintained in the Operetta CLS Live Cell Analysis System to monitor cell confluence for 120 h.

Cell apoptosis/necrosis was examined by Annexin V-FITC/PI staining. B16F10 cells were seeded in 12-well plates ($10^5$ cells/well) for 24 h. Thereafter, cells were transfected with TPCS@EV for 4 h (siPAK4, 100 nmol/L). Cells in the photo-treatment group were subjected to 660 nmol/L laser irradiation (0.1 W/cm$^2$, 2 min). After incubation for another 44 h, cells were stained with Annexin V-FITC/PI for flow cytometry (FCM) analysis.

### 2.9. Antitumor synergism in vitro and in vivo

Next, we quantitatively determined whether the antitumor effects between PAK4 silencing and immunogenic phototherapy were synergistic, additive, or antagonistic *in vitro* by using the CompuSyn method. To achieve individual immunogenic phototherapy without PAK4 silencing, the TPC polymer was complexed with siNC to prepare TPCS$^{siNC}$@EV nanoparticles. Accordingly, to achieve a combined effect between PAK4 silencing and immunogenic phototherapy, TPCS@EV nanoparticles were used. As full PAK4 silencing can only be achieved in the presence of photo-treatment, it is impossible to measure the individual contribution of PAK4 silencing for TPCS@EV. A1-D1-5-based ionizable lipid nanoparticle termed "iLAND" was developed by our group and has been shown to work well for siRNA delivery *in vitro* and *in vivo*[33]. In addition, iLAND/siPAK4 complexes (iLAND$^{siPAK4}$) showed a comparable knockdown efficiency to that of TPCS@EV *in vitro* and *in vivo* (Supporting Information Fig. S1). Therefore, iLAND$^{siPAK4}$ was used to achieve individual PAK4 silencing without phototherapy instead of TPCS@EV. B16F10 and CT26-Luc cells were transfected with iLAND$^{siPAK4}$ at the siPAK4 concentrations of 1.0, 2.0, 3.0, 4.0, 5.0, 7.5, 10.0, 12.5 and 15.0 μg/mL. Accordingly, cells were individually transfected with TPCS$^{siNC}$@EV nanoparticles plus photo-treatment (TPCS$^{siNC}$@EV L+) and TPCS@EV nanoparticles plus photo-treatment (TPCS@EV L+) at the siRNA concentrations of 1, 2.5, 5.0, 7.5, 10.0, 12.5 and 15.0 μg/mL. Cells in photo-treatment groups were exposed to 660 nmol/L laser irradiation (0.1 W/cm$^2$, 2 min). After incubation for 48 h, cell viability was determined by using the MTT assay. Specifically, 20 μL of MTT solution (5 mg/mL) was added to each well followed by incubation for 4 h. The culture medium was then replaced with 200 μL of dimethyl sulfoxide to dissolve the formed formazan crystals, and the absorbance of the formazan solution was measured at 490 nmol/L by using a SpectraMax M3 microplate reader (Molecular Devices). Finally, the antitumor efficiency was determined and subjected to synergistic analysis using the CompuSyn method.

To investigate the antitumor synergism *in vivo*, C57BL/6J mice were implanted with B16F10 cells as described in section 2.7. When the tumor volume reached approximately 80 mm$^3$, mice were intravenously injected with TPCS$^{siNC}$@EV L+, TPCS@EV L+, or iLAND$^{siPAK4}$ at different siRNA doses (*i.e.*, 0.25, 0.5, and 1 mg/kg) once every other day for a total of 4 injections ($n = 5$). After 8 h post-injection, mice in photo-treatment groups were exposed to 660 nmol/L laser irradiation (0.2 W/cm$^2$, 10 min) at the tumor sites. The tumor size and body weight were measured every other day. On Day 22, the tumor tissues were excised and weighed. The tumor volume and tumor weight in TPCS$^{siNC}$@EV L+, TPCS@EV L+, and iLAND$^{siPAK4}$ treated groups at different doses were compared to the PBS-treated group to calculate the reduction of tumors. The percent reductions of tumor volume and tumor weight were then subjected to synergism and dose reduction analysis by using the CompuSyn method. To evaluate the biocompatibility of TPCS$^{siNC}$@EV L+, TPCS@EV L+, and iLAND$^{siPAK4}$, the major organs, including the brain, heart, liver, spleen, lung, and kidney of mice receiving the highest siRNA doses were collected for Hematoxylin and Eosin (H&E) staining.

### 2.10. Statistical analysis

Two-tailed Student's *t*-test was utilized to analyze the significant difference between the two groups, while the analysis of variance (ANOVA) was used to perform multiple comparisons. Results are presented as mean ± standard deviation (SD). A $P$ value less than 0.05 was considered statistically significant with $^*P < 0.05$, $^{**}P < 0.01$, $^{***}P < 0.001$, and $^{****}P < 0.0001$, respectively.

## 3. Results

### 3.1. Preparation and characterization of the engineered EVs

EVs were isolated from the culture medium of M1 macrophages through ultracentrifugation. Western blot, TEM imaging, and NTA results confirmed the successful isolation of EVs (Fig. 2A–C). Besides, the isolated EVs significantly expressed some proinflammatory markers of M1 macrophages, such as CD80, MHCII, and Ly6C (Supporting Information Fig. S2). The *in vivo* fluorescence imaging result revealed the tumor tropism of M1 macrophage-derived EVs (Supporting Information Fig. S3). The Ce6-conjugated, thioketal-linked polyethyleneimine (TPC) previously developed by our group was used to complex with siPAK4 to form the TPCS nano-complexes[32]. Subsequently, the TPCS nano-complex cores were encapsulated by EVs through the extrusion approach to generate the engineered EVs (TPCS@EV). The optimal weight ratio between EVs and TPC was 1:1, TPCS@EV prepared at the weight ratio had the lowest particle size (Supporting Information Fig. S4). Confocal laser scanning microscopy (CLSM) and NanoView images of TPCS@EV revealed an obvious overlap of the fluorescent signals of EVs and TPCS nano-complex cores (Fig. 2D and E). Additionally, the SDS-PAGE image revealed that TPCS@EV presented a similar protein expression pattern to that of EVs (Supporting Information Fig. S5). Compared to TPCS, TPCS@EV displayed a round, core–shell structure (Fig. 2F). Following surface coating, the average hydrodynamic diameter of nanoparticles increased from about 100 nmol/L of the uncoated TPCS to about 117 nmol/L of the coated TPCS@EV. Accordingly, the surface charge decreased significantly from about 16 mV of TPCS to about −7 mV of TPCS@EV (Fig. 2G). These results collectively confirm the encapsulation of EVs on TPCS nano-complexes. Both TPCS and TPCS@EV nanoparticles exhibited good stability without significant change in the average particle size after storing at room temperature away from light for 24 h (Supporting Information Fig. S6). PCS@EV could effectively load siRNA with an encapsulation efficiency of 93.4%, which was comparable to that of Lipo 2000, a commercial transfection reagent (Supporting Information Fig. S7). After that, we explored the ROS-responsive property of TPCS@EV and confirmed that TPCS@EV could disassemble into a relatively smaller irregular structure and released siPAK4 following laser irradiation, likely due to the cleavage of ROS-sensitive thioketal linkers (Fig. 2F and Supporting Information Fig. S8A and B). TPCS@EV exhibited better tumor accumulation *in vivo* than TPCS, revealing that EV coating considerably improved the targeting capability (Supporting Information Fig. S9).

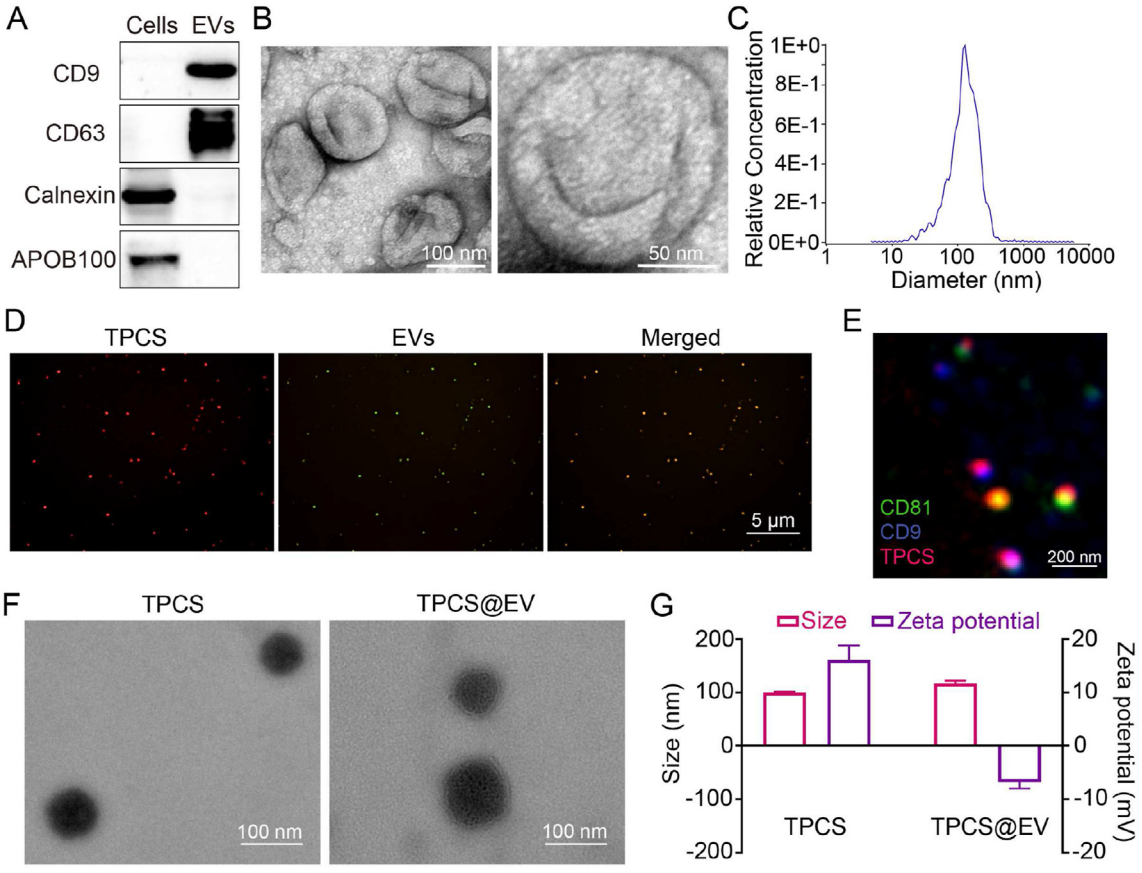


**Figure 2** Preparation and characterization of the engineered EVs (TPCS@EV). (A) Western blot analysis of the positive markers (*i.e.*, CD9 and CD63) and negative markers (*i.e.*, calnexin and APOB100) of M1 macrophage-derived EVs. TEM imaging (B) and nanoparticle tracking analysis (C) of EVs. (D) Fluorescence colocalization analysis of TPCS@EV by CLSM. Red, TPCS nano-complexes. Green, 3,3−dioctadecyloxacarbocyanine perchlorate (DiO)-labeled EVs. (E) Fluorescence colocalization analysis of TPCS@EV by NanoView. Red, TPCS. Green, CD81-positive EVs. Blue, CD9-positive EVs. TEM imaging (F) and dynamic light scattering analysis (G) of TPCS and TPCS@EV. Data in G are represented as mean ± SD ($n = 3$).

### *3.2. PAK4 silencing and immunogenic cell death (ICD) cascade in vitro and in vivo*

The ability of the engineered EVs to induce PAK4 silencing and immunogenic cell death (ICD) cascade was examined. As shown in Fig. 3A, the level of PAK4 mRNA and protein in B16F10 cells was significantly downregulated after being treated with TPCS@EV plus laser irradiation (TPCS@EV L+), when compared to the PBS, siPAK4, TPCS$^{siNC}$@EV plus laser irradiation (TPCS$^{siNC}$@EV L+) and TPCS@EV without laser irradiation (TPCS@EV L-) treated groups ($P < 0.01$). Compared to TPCS L+ treatment, a slight, but not significant, increase in silencing efficiency *in vitro* was observed for TPCS@EV L+. Moreover, the mRNA and protein level of PAK4 in the tumor tissue of B16F10 tumor-bearing mice was further investigated. Likewise, a significant improvement in silencing potency was observed for TPCS@EV L+ treatment in comparison to siPAK4, TPCS$^{siNC}$@EV L+, and TPCS@EV L-treatments ($P < 0.001$). Of note, TPCS@EV L+ exhibited higher knockdown efficiency *in vivo* than TPCS EV L+ ($P < 0.05$), possibly due to the enhanced tumor targeting ability (Fig. 3B).

As the generation of ROS is essential for the induction of the ICD cascade, the capacity of TPCS@EV to enhance the level of intracellular ROS in response to laser irradiation was examined. It was observed that similar to TPCS L+, TPCS@EV L+ effectively induced the generation of intracellular ROS (Supporting Information Fig. S10). We then tested whether the photoactivatable EVs could induce an ICD cascade by measuring CRT exposure, HMGB1 release, and ATP secretion. CLSM images and western blot results validated that TPCS@EV effectively boosted CRT exposure in the presence of laser irradiation (Fig. 3C and D). Besides, the release of HMGB1 and ATP in the culture medium was significantly enhanced after TPCS@EV L+ treatment (Fig. 3E and F). To evaluate the ICD cascade *in vivo*, the tumor tissues of B16F10 tumor-bearing mice after various treatments were collected for immunofluorescence analysis of CRT exposure. Compared to other groups, TPCS@EV plus laser irradiation boosted higher CRT exposure in the tumor tissues, which was in agreement with the result of PAK4 silencing *in vivo* (Fig. 3G). Taken together, EV encapsulation and laser irradiation enhanced the PAK4 silencing and ICD cascade of TPCS@EV *in vivo*.

### *3.3. Antitumor activity of the engineered EVs*

Having proven TPCS@EV L+ could induce potent PAK4 silencing and ICD cascade, we then tested whether the engineered EVs could elicit effective antitumor activity. First, the ability of TPCS@EV to inhibit the proliferation of tumor cells was

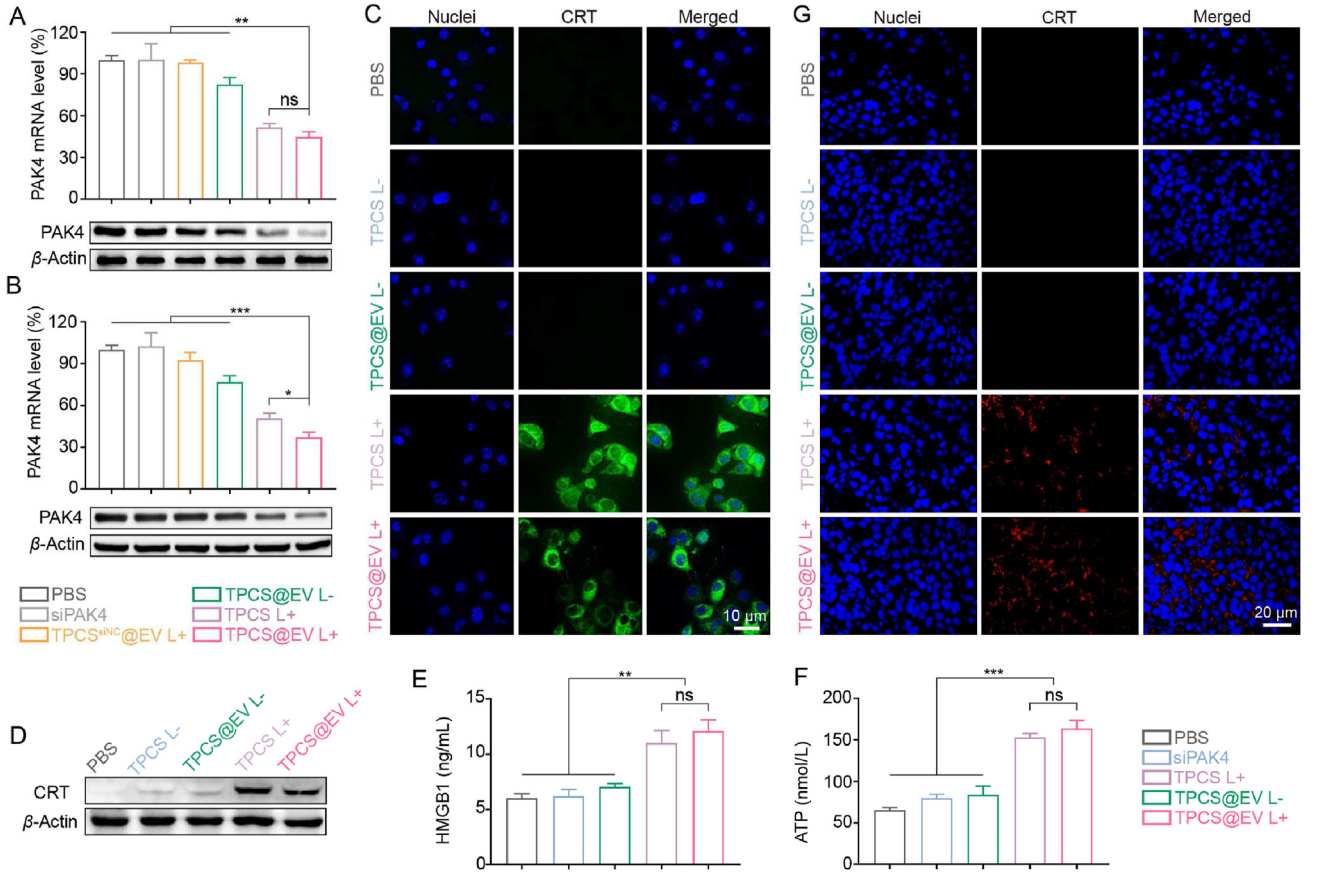


**Figure 3** The engineered EVs (TPCS@EV) induced potent PAK4 silencing and immunogenic phototherapy *in vitro* and *in vivo*. The PAK4 mRNA and protein level in B16F10 cells (A) and the tumor tissues of B16F10 tumor-bearing mice (B) after various treatments. For the $TPCS^{siNC}$@EV complex, TPC was complexed with siNC instead of siPAK4. Fluorescence imaging (C) and Western blot analysis (D) of calreticulin (CRT) exposure in B16F10 cells after different treatments. Determination of high mobility group box 1 protein (HMGB1) release (E) and adenosine triphosphate (ATP) secretion (F) in the culture media of B16F10 cells following different treatments by using ELISA and ATP assay, respectively. (G) Fluorescence imaging of CRT exposure in the tumor tissues of B16F10 tumor-bearing mice after different treatments. Data in A, B, E, and F are represented as mean ± SD ($n = 3$) *$P < 0.05$, **$P < 0.01$, ***$P < 0.001$. ns, not significant.

examined by measuring cell confluence using the Operetta CLS Live Cell Analysis System. Compared to the untreated cells, TPCS@EV plus laser irradiation effectively inhibited the proliferation of B16F10 by 82.6%. In contrast, TPCS@EV without photo-treatment exhibited no significant inhibition of cell proliferation (Fig. 4A and B). The results suggest laser irradiation was of key importance to enhance the antiproliferative activity of TPCS@EV. Similarly, an effective antiproliferative efficiency of 67.6% was observed in CT26-Luc cells after treating cells with TPCS@EV in the presence of photo-treatment (Fig. 4C and D). Additionally, the capacity of TPCS@EV to induce cell apoptosis and necrosis was measured. As shown in Supporting Information Fig. S11, TPCS@EV plus laser irradiation could significantly promote the apoptosis and necrosis of B16F10 cells, when compared to the PBS and TPCS@EV L-groups.

### 3.4. *Synergistic antitumor effects in vitro*

The synergistic antitumor activity of TPCS@EV in B16F10 and CT26-Luc cells was examined. As shown in Fig. 5A and B, TPCS@EV combined PAK4 silencing with immunogenic phototherapy, thus contributing to higher cancer cell-killing activity than PAK4 silencing and immunogenic phototherapy treatment alone. In addition, the antitumor synergism between PAK4 silencing and immunogenic phototherapy was quantitatively determined by using the CompuSyn method. The combination index (CI) values $<1$, $=1$, and $>1$ indicate synergism, additive effect, and antagonism, respectively[34]. The CompuSyn analysis result indicates that the CI values for the combined treatment of TPCS@EV were $<1$ in B16F10 and CT26-Luc cells, revealing there was a synergistic antitumor effect between PAK4 silencing and phototherapy *in vitro* (Fig. 5C and D).

### 3.5. *Synergistic antitumor effects in vivo*

We further investigated whether the combined antitumor therapy between PAK4 silencing and immunogenic phototherapy of TPCS@EV *in vivo* was synergistic, additive, or antagonistic. As shown in Fig. 6A–C and Supporting Information Fig. S12, mice receiving the combined treatment showed slower tumor growth, smaller tumor size, and lower tumor weight than mice receiving PAK4 silencing or immunogenic phototherapy treatment alone. The anticancer activity of the combined treatment of TPCS@EV was further confirmed by H&E staining of the excised tumor

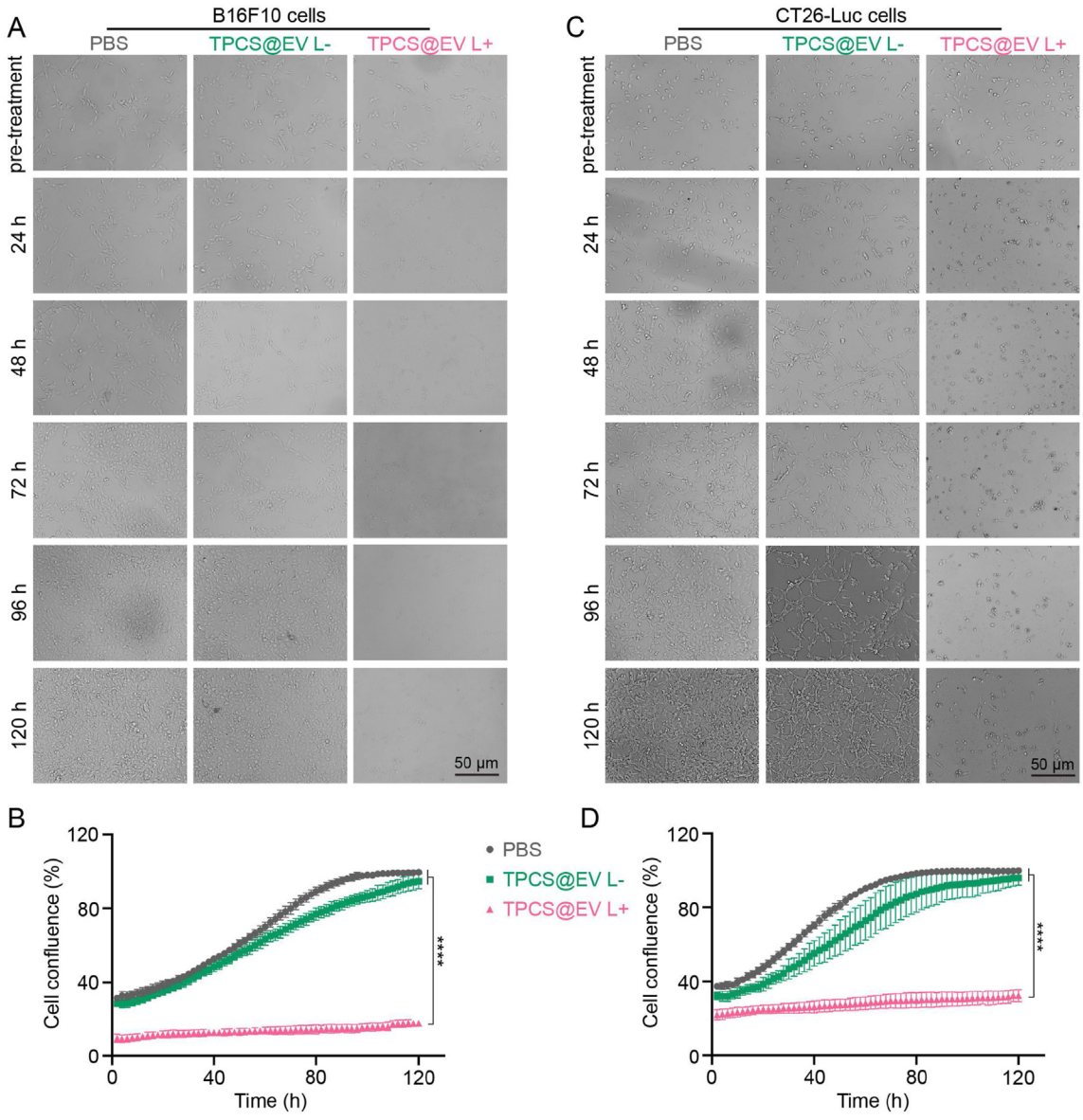


**Figure 4** The antiproliferative effects of the engineered EVs (TPCS@EV) with or without photo-treatment in B16F10 and CT26-Luc cells. Cell proliferation was examined by using the Operetta CLS Live Cell Analysis System. Bright-field imaging (A) and cell confluence determination (B) of B16F10 cells after various treatments. Bright-field imaging (C) and cell confluence determination (D) of CT26-Luc cells after various treatments. Data in B and D are represented as mean ± SD ($n = 3$), ****$P < 0.0001$.

tissues (Fig. 6D). As shown by the results of CompuSyn analysis, the combination index (CI) values for the combined treatment against tumor volume on Days 16, 18, 20, and 22 were <1 at the higher level (Fig. 6E and Table S1). Besides, all the CI values for the combined treatment against the tumor weight were <1 (Fig. 6F). Together, these results confirm that there were synergistic antitumor effects on inhibition of tumor growth (*i.e.*, tumor volume and tumor weight) for the combined treatment of TPCS@EV.

In line with the CI values, isobolograms for 50%, 75%, and 90% inhibition of tumor volume demonstrated that the combined treatment at $ED_{50}$, $ED_{75}$, and $ED_{90}$ showed antitumor synergism, which occurred at a higher level and in the latter stage of the treatment (Supporting Information Fig. S13). Moreover, it is indicated that the dose reduction index (DRI) >1, =1, and <1 indicates favorable dose reduction, no dose reduction, and unfavorable dose reduction, respectively[34,35]. All the DRI values for the combined treatment of TPCS@EV against tumor volume on Days 16, 18, 20, and 22 were >1, indicating there was a favorable dose reduction between PAK4 silencing and immunogenic phototherapy (Supporting Information Fig. S14 and Table S1). In addition, the antitumor synergism and favorable dose reduction values for the combined treatment were agreed to the results of the CompuSyn simulation of tumor weight (Supporting Information Fig. S15A and S15B). For $ED_{95}$ on Day 22, the DRI value indicated PAK4 silencing (*i.e.*, siPAK4) dose can be reduced by about 6.07-folds and immunogenic phototherapy (*i.e.*, TPC) dose can be reduced by 2.15-folds in the combined treatment, when compared to the $ED_{50}$ value of each therapy alone (Table S1).

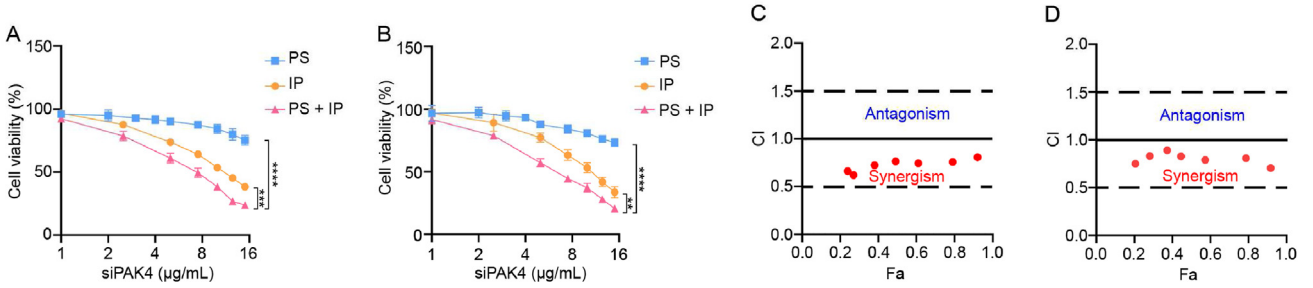


**Figure 5** The synergistic antitumor activity between PAK4 silencing and immunogenic phototherapy of the engineered EVs in B16F10 and CT26-Luc cells. The cell viability of B16F10 (A) and CT26-Luc (B) cells after being treated with individual PAK4 silencing (PS), individual immunogenic phototherapy (IP), and the combined treatment between PAK4 silencing and immunogenic phototherapy (PS + IP). The combination index (CI) of the combined treatment between PAK4 silencing and immunogenic phototherapy in B16F10 cells (C) and CT26-Luc cells (D). Fa, Fraction affected. CI values <1, =1, and >1 indicate synergism, additive effect, and antagonism, respectively. Data in A and B are represented as mean ± SD ($n = 3$). $^{**}P < 0.01$, $^{***}P < 0.001$, $^{****}P < 0.0001$.

The biocompatibility properties of individual PAK4 silencing, individual immunogenic phototherapy, and the combined treatment were assessed. The results show that there was no significant alteration of body weight in different groups at the highest siRNA dose (Supporting Information Fig. S16). In addition, no obvious histological toxicity and inflammation infiltrates were observed in major organs of mice, including the brain, heart, liver, spleen, lung, and kidney, after different treatments at the highest siRNA

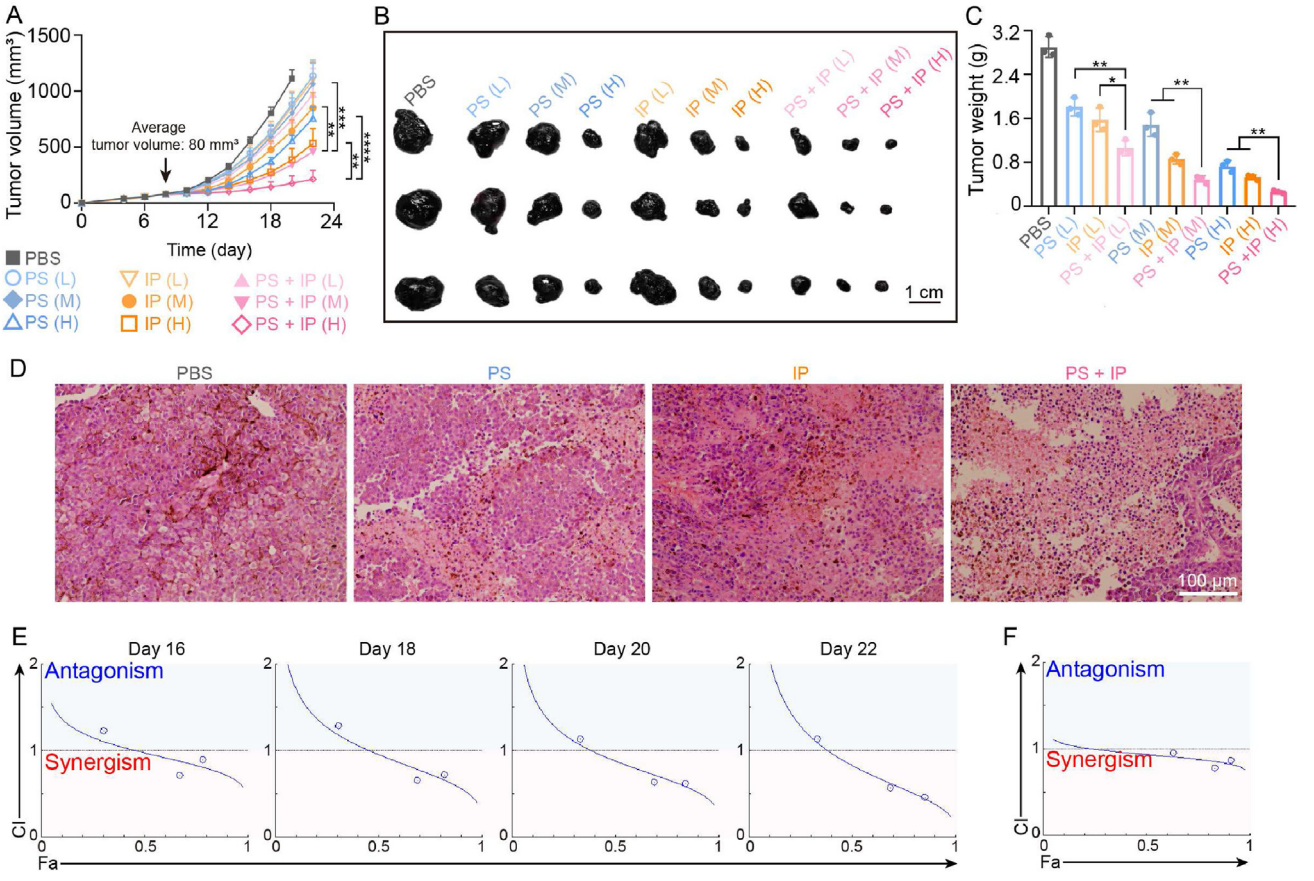


**Figure 6** The antitumor synergism between PAK4 silencing and immunogenic phototherapy of the engineered EVs in B16F10 tumor-bearing mice at different siRNA doses (L, 0.25 mg/kg; M, 0.5 mg/kg; H, 1 mg/kg). The average tumor growth curves (A) ($n = 5$), and the representative images (B) and weight (C) of the excised tumors after different treatments ($n = 3$). (D) Representative images of Hematoxylin and Eosin (H&E) staining of the excised tumors. The combination index (CI) for the combined treatment against tumor volume on different dates (E) and against tumor weight (F), as determined by using the CompuSyn method. PS, individual PAK4 silencing. IP, individual immunogenic phototherapy. PS + IP, the combined treatment between PAK4 silencing and immunogenic phototherapy. Fa, Fraction affected. Data in A and C are represented as mean ± SD. $^{*}P < 0.05$, $^{**}P < 0.01$, $^{***}P < 0.001$, $^{****}P < 0.0001$.

doses (Supporting Information Fig. S17). These results collectively confirm the biosafety of the combined treatment of TPCS@EV.

## 4. Discussion

Overexpression of PAK4 in cancer cells has multiple oncogenic signaling, such as the acquisition of proliferation, survival, and invasion. More recently, PAK4 has been identified as a key regulator of the phosphorylation and nuclear translocation of $\beta$-catenin, thus leading to the activation of Wnt/$\beta$-catenin signaling and immune evasion in cancers such as melanoma and colorectal carcinoma[10,11]. To this end, PAK4 silencing holds great potential for cancer treatment to directly inhibit cancer proliferation and promote immune infiltration. Currently, PAK4 has been widely adopted as a drug target, and several PAK4 inhibitors (*i.e.*, KPT-9274, ATG-019, and PF-03758309) are in clinical trials such as NCT04281420, NCT00932126, NCT04914845, and NCT02702492[36].

Compelling pieces of evidence validated that phototherapy can induce immunogenic cell death (ICD) by utilizing photosensitizer agents to adsorb near-infrared laser and release ROS[13,14]. Apart from directly killing cancer cells, immunogenic phototherapy is capable of promoting the release of damage-associated molecular patterns (DAMPs). As a stimulatory signal, DAMPs can increase tumor immunogenicity and activate the immune system by promoting dendritic cell maturation and antigen presentation, which eventually primes the naïve T cells into $CD8^+$ cytotoxic T cells[13,15]. Therefore, immunogenic phototherapy holds great promise to induce immune activation in combined cancer immunotherapy.

Herein, we established a combined antitumor modality by combining PAK4 silencing with immunogenic phototherapy using engineered EVs for synergistically-boosted antitumor efficacy. The antitumor synergism was quantitatively determined by using the CompuSyn approach. The combination index (CI) demonstrated that there were synergistic antitumor effects between PAK4 silencing and immunogenic phototherapy of TPCS@EV *in vitro* and *in vivo*. The antitumor synergism *in vivo* occurred at higher siRNA doses and in the latter stages of the scheduled therapy. Slight antagonism was observed for the combined treatment at a lower level (*i.e.*, lower fa value). This is of less concern since CI values are less relevant to the therapeutic outcome at a low level. By contrast, synergism or antagonism is more important and therapeutically relevant at high dose levels for cancer treatment, as fighting cancer in small fractions has slight significance in cancer treatment[34,37]. The dose reduction index (DRI) analysis revealed favorable dose reductions for the combined treatment between PAK4 silencing and immunogenic phototherapy. These dose reductions may contribute to lower toxicity and higher biocompatibility[35]. Taken together, our results demonstrated that the engineered EVs achieved synergistic antitumor effects between PAK4 silencing and immunogenic phototherapy.

## 5. Conclusions

In summary, the engineered EVs were established to combine PAK4 silencing with immunogenic phototherapy for synergistic antitumor outcomes. The engineered EVs induced robust PAK4 silencing and ICD cascade *in vitro* and *in vivo*. As a consequence, effective inhibition of the proliferation and growth of cancer cells was achieved. Moreover, the synergistic antitumor effect of the combined treatment was quantitatively demonstrated *in vitro* and *in vivo*, revealing that the combined treatment was more effective than PAK4 silencing and immunogenic phototherapy alone. Together, the study presents a synergistically potentiated cancer treatment modality by combining PAK4 silencing with immunogenic phototherapy in the engineered EVs, which is essential and promising for synergistic antitumor treatment.

## Acknowledgments

The authors thank the National Natural Science Foundation of China (32101157, 82104105, 31871003, 32171394, 32030060), National Key Research & Development Program of China (2021YFA1201000, 2021YFE0106900, 2021YFC2302400, 2018YFE0117800), the Fundamental Research Funds for the Central Universities (2022CX01013, China), and China Postdoctoral Science Foundation (2021M693966). The authors thank the Biological and Medical Engineering Core Facilities, and Analysis & Testing Center (Beijing Institute of Technology) for supporting experimental equipment (China).

## Author contributions

Mei Lu, Haonan Xing, Xing-Jie Liang, and Yuanyu Huang designed the research. Mei Lu and Haonan Xing carried out the experiments. Wanxuan Shao, Pengfei Wu, and Yuchuan Fan provided experimental assistance. Mei Lu, Haonan Xing, Xing-Jie Liang, and Yuanyu Huang analyzed the data. Mei Lu and Haonan Xing wrote the manuscript. Xing-Jie Liang and Yuanyu Huang revised the manuscript. Huining He, Stefan Barth, and Aiping Zheng were involved in the discussion. All of the authors have read and approved the final manuscript.

## Conflicts of interest

The patents related to the study have been filed by Mei Lu, Haonan Xing, Xing-Jie Liang, and Yuanyu Huang. The other authors declare no conflicts of interest.

## Appendix A. Supporting information

Supporting data to this article can be found online at https://doi.org/10.1016/j.apsb.2023.03.020.

## References

1. Kim TK, Vandsemb EN, Herbst RS, Chen L. Adaptive immune resistance at the tumour site: mechanisms and therapeutic opportunities. *Nat Rev Drug Discov* 2022;**21**:529–40.
2. Nam J, Son S, Park KS, Zou W, Shea LD, Moon JJ. Cancer nanomedicine for combination cancer immunotherapy. *Nat Rev Mater* 2019;**4**:398–414.
3. Zhang J, Sun X, Zhao X, Yang C, Shi M, Zhang B, et al. Combining immune checkpoint blockade with ATP-based immunogenic cell death amplifier for cancer chemo-immunotherapy. *Acta Pharm Sin B* 2022;**12**:3694–709.
4. Xu Y, Xiong J, Sun X, Gao H. Targeted nanomedicines remodeling immunosuppressive tumor microenvironment for enhanced cancer immunotherapy. *Acta Pharm Sin B* 2022;**12**:4327–47.
5. Zhu SM, Zhang T, Zheng L, Liu HT, Song WR, Liu DL, et al. Combination strategies to maximize the benefits of cancer immunotherapy. *J Hematol Oncol* 2021;**14**:156.

6. Spranger S, Bao R, Gajewski TF. Melanoma-intrinsic $\beta$-catenin signalling prevents anti-tumour immunity. *Nature* 2015;**523**:231−5.
7. Sharma P, Hu-Lieskovan S, Wargo JA, Ribas A. Primary, adaptive, and acquired resistance to cancer immunotherapy. *Cell* 2017;**168**:707−23.
8. Kumar R, Gururaj AE, Barnes CJ. p21-activated kinases in cancer. *Nat Rev Cancer* 2006;**6**:459−71.
9. Radu M, Semenova G, Kosoff R, Chernoff J. PAK signalling during the development and progression of cancer. *Nat Rev Cancer* 2014;**14**:13−25.
10. Gajewski TF, Fessler J. PAK4 as a cancer immune-evasion target. *Nat Cancer* 2020;**1**:18−9.
11. Abril-Rodriguez G, Torrejon DY, Liu W, Zaretsky JM, Nowicki TS, Tsoi J, et al. PAK4 inhibition improves PD-1 blockade immunotherapy. *Nat Cancer* 2020;**1**:46−58.
12. Galluzzi L, Buqué A, Kepp O, Zitvogel L, Kroemer G. Immunogenic cell death in cancer and infectious disease. *Nat Rev Immunol* 2017;**17**:97−111.
13. Ng CW, Li J, Pu K. Recent progresses in phototherapy-synergized cancer immunotherapy. *Adv Funct Mater* 2018;**28**:1804688.
14. Krysko DV, Garg AD, Kaczmarek A, Krysko O, Agostinis P, Vandenabeele P. Immunogenic cell death and DAMPs in cancer therapy. *Nat Rev Cancer* 2012;**12**:860−75.
15. Shi Y, Lammers T. Combining nanomedicine and immunotherapy. *Acc Chem Res* 2019;**52**:1543−54.
16. Lu M, Xing H, Zheng A, Huang Y, Liang X-J. Overcoming pharmaceutical bottlenecks for nucleic acid drug development. *Acc Chem Res* 2023;**56**:224−36.
17. Lu M, Shao W, Xing H, Huang Y. Extracellular vesicle-based nucleic acid delivery. *Interdiscip Med* 2023;**1**:e20220007.
18. Michaela S, Aigner A. Nucleic acid delivery with extracellular vesicles. *Adv Drug Deliver Rev* 2021;**173**:89−111.
19. Lu M, Xing H, Xun Z, Yang T, Ding P, Cai C, et al. Exosome-based small RNA delivery: progress and prospects. *Asian J Pharm Sci* 2018;**13**:1−11.
20. Lu M, Huang Y. Bioinspired exosome-like therapeutics and delivery nanoplatforms. *Biomaterials* 2020;**242**:119925.
21. Guo S, Li K, Hu B, Li C, Zhang M, Hussain A, et al. Membrane-destabilizing ionizable lipid empowered imaging-guided siRNA delivery and cancer treatment. *Exploration* 2021;**1**:35−49.
22. Liu J, Chen C, Wei T, Gayet O, C L, Borge L, et al. Dendrimeric nanosystem consistently circumvents heterogeneous drug response and resistance in pancreatic cancer. *Exploration* 2021;**1**:21−34.
23. Liu HL, Huang LL, Mao MC, Ding JJ, Wu GH, Fan WL, et al. Viral protein-pseudotyped and siRNA-electroporated extracellular vesicles for cancer immunotherapy. *Adv Funct Mater* 2020;**30**:2006515.
24. Mills CD, Lenz LL, Harris RA. A breakthrough: macrophage-directed cancer immunotherapy. *Cancer Res* 2016;**76**:513−6.
25. Lu M, Xing H, Xun Z, Yang T, Zhao X, Cai C, et al. Functionalized extracellular vesicles as advanced therapeutic nanodelivery systems. *Eur J Pharm Sci* 2018;**121**:34−46.
26. Lu M, Xing H, Yang Z, Sun Y, Yang T, Zhao X, et al. Recent advances on extracellular vesicles in therapeutic delivery: challenges, solutions, and opportunities. *Eur J Pharm Biopharm* 2017;**119**:381−95.
27. Johnsen KB, Gudbergsson JM, Duroux M, Moos T, Andresen TL, Simonsen JB. On the use of liposome controls in studies investigating the clinical potential of extracellular vesicle-based drug delivery systems − a commentary. *J Control Release* 2018;**269**:10−4.
28. Lu M, Zhao X, Xing H, Xun Z, Zhu S, Lang L, et al. Comparison of exosome-mimicking liposomes with conventional liposomes for intracellular delivery of siRNA. *Int J Pharm* 2018;**550**:100−13.
29. Lu M, Zhao X, Xing H, Liu H, Lang L, Yang T, et al. Cell-free synthesis of connexin 43-integrated exosome-mimetic nanoparticles for siRNA delivery. *Acta Biomater* 2019;**96**:517−36.
30. Lu M, Zhao X, Xing H, Xun Z, Yang T, Cai C, et al. Liposome-chaperoned cell-free synthesis for the design of proteoliposomes: implications for therapeutic delivery. *Acta Biomater* 2018;**76**:1−20.
31. Cheng G, Li W, Ha L, Han X, Hao S, Wan Y, et al. Self-assembly of extracellular vesicle-like metal-organic framework nanoparticles for protection and intracellular delivery of biofunctional proteins. *J Am Chem Soc* 2018;**140**:7282−91.
32. Lu M, Xing H, Shao W, Zhang T, Zhang M, Wang Y, et al. Photoactivatable silencing extracellular vesicle (PASEV) sensitizes cancer immunotherapy. *Adv Mater* 2022;**34**:2204765.
33. Hu B, Li B, Li K, Liu YY, Li CH, Zheng LL, et al. Thermostable ionizable lipid-like nanoparticle (iLAND) for RNAi treatment of hyperlipidemia. *Sci Adv* 2022;**8**:eabm1418.
34. Chou TC. Theoretical basis, experimental design, and computerized simulation of synergism and antagonism in drug combination studies. *Pharmacol Rev* 2006;**58**:621−81.
35. Fu J, Zhang N, Chou JH, Dong H-J, Lin S-F, Ulrich-Merzenich GS, et al. Drug combination in vivo using combination index method: taxotere and T607 against colon carcinoma HCT-116 xenograft tumor in nude mice. *Synergy* 2016;**3**:15−30.
36. Abu Aboud O, Chen CH, Senapedis W, Baloglu E, Argueta C, Weiss RH. Dual and specific inhibition of NAMPT and PAK4 by KPT-9274 decreases kidney cancer growth. *Mol Cancer Ther* 2016;**15**:2119−29.
37. Chou TC. Drug combination studies and their synergy quantification using the Chou-Talalay method. *Cancer Res* 2010;**70**:440−6.